Long-range exchange interaction in triple quantum dots in the Kondo regime

YongXi Cheng,[1,2] YuanDong Wang,[1] JianHua Wei,[1,*] ZhenGang Zhu,[3] and YiJing Yan[4,5]

[1]*Department of Physics, Renmin University of China, Beijing 100872, China*

[2]*Department of Science, Taiyuan Institute of Technology, Taiyuan 030008, China*

[3]*School of Electronic, Electrical and Communication Engineering, University of Chinese Academy of Sciences, Beijing 100049, China*

[4]*Hefei National Laboratory for Physical Sciences at the Microscale, University of Science and Technology of China, Hefei, Anhui 230026, China*

[5]*Department of Chemistry, Hong Kong University of Science and Technology, Kowloon, Hong Kong*

(Received 1 August 2016; revised manuscript received 30 March 2017; published 12 April 2017)

Long-range interactions in triple quantum dots in the Kondo regime are investigated by accurately solving the three-impurity Anderson model. For the occupation configuration of $(N_1,N_2,N_3) = (1,0,1)$, a long-range antiferromagnetic exchange interaction (J_{AF}) is demonstrated and induces a crossover from the separated Kondo singlet to the long-range spin singlet state between edge dots. In the long-range spin singlet phase, a long-range overlapping or entanglement of Kondo clouds is discovered, which induces a transition peak in the spectral function of the middle dot under equilibrium conditions. Under nonequilibrium conditions, the long-range entanglement of the Kondo clouds is characterized by the conductance peak at zero bias, which can be observed in experiments.

DOI: 10.1103/PhysRevB.95.155417

I. INTRODUCTION

Long-range interaction as a high-order interaction originates from the superpositions of indirectly coupled states. It plays an important role in many-body physics and quantum computing [1–4]. For the latter, the long-range interaction makes it possible to manipulate a distant quantum gate or qubit in one step, which is of higher operating efficiency and fault-tolerant capability than nearest-neighbor control in exchange-based quantum gates [5]. The triple-quantum-dot (TQD) device provides an ideal platform for investigating the quantum manipulation [6–11]. The long-range transport in serially coupled TQDs has been observed in recent experiments [3,12,13]. For example, Platero *et al.* measured a resonant transport line (in the area of the bipolar spin blockade) between the edge dots, which suggests a long-range coherent superposition near the degenerate point of $(N_1,N_2,N_3) = (1,1,1)/(2,1,2)$ (N_i is the number of electrons in ith QD) [12]. Shortly afterwards, the same group reported a long-range spin transfer near another degenerate point of $(1,0,1)/(2,0,2)$, where QD2 remains unoccupied during the tunneling process [13]. Vandersypen *et al.* demonstrated a high-order coherent tunneling between QD1 and 3 near the degenerate point of $(0,1,0)/(1,1,1)$ through the observation of Landau-Zener-Stückelberg interference [3].

In order to produce measurable current, all of above experimental results are achieved in the boundary of Coulomb blockade near degenerate points in the stability diagram. However, these regimes are not suitable for theoretical analysis of the long-range interaction (especially the long-range spin correlation or exchange interaction), since occupation numbers and magnetic moments of QD1 and 3 are not conserved during the transport under bias in those boundaries. One better choice is to push the range of study deeply into the Coulomb blockade region far away from the degenerate points, such as the local moment regime of QD1 and 3 where both the occupation number and spin are well defined. In order to produce measurable current or other observable features, we investigate the long-range exchange interaction and its effects in the Kondo regime.

The Kondo phenomenon itself is an important and interesting issue in TQDs. It results from the screening of a localized spin by the delocalized spins from reservoirs (or leads), which presents a pronounced zero-bias conductance peak at temperatures below the Kondo temperature in QD systems, with a Kondo singlet (KS) formed [14–16]. Recently considerable theoretical efforts have been made in the topic of serial TQDs, such as the equilibrium and nonequilibrium Kondo transport properties [17], Fermi-liquid versus non-Fermi-liquid behavior [18], and two-channel Kondo physics [19]. In addition, the Kondo phenomenon in other structures of TQDs has been discussed as well, including the mirror symmetry TQDs [20–22], triangular TQDs [23–26], and parallel TQDs [27]. To the best of our knowledge, none of these works concern the long-range exchange interaction and its effect on the Kondo phenomenon in TQDs.

In the present work, we study the long-range exchange interaction between QD1 and 3 in the Kondo regime in serial TQDs, by accurately solving the three-impurity Anderson model with the hierarchical equation of motion (HEOM) formalism [28,29]. The geometry is depicted in Fig. 1(a). Two symmetrical edge dots (QD1 and 3) are in the local magnetic moment regime ($N_1 = N_3 = 1$), and are coupled to the source (S) and drain (D) reservoir but decoupled from each other ($t_{13} = 0$). The intermediate one (QD2) symmetrically couples to the QD1 and 3 ($t_{12} = t_{23} = t$) via a variable singly occupied level ε_2 modulated by a gate voltage V_g. In order to highlight the long-range correlation, we focus on the occupation configuration of $(N_1,N_2,N_3) = (1,0,1)$ by pushing ε_2 high enough, as schematically shown in Fig. 1(b). In the limit of $(1,1,1)$, we have reported a reappearance of the Kondo phenomenon and worked out an effective ferromagnetic exchange interaction between QD1 and 3 [30]. In the present

*wjh@ruc.edu.cn

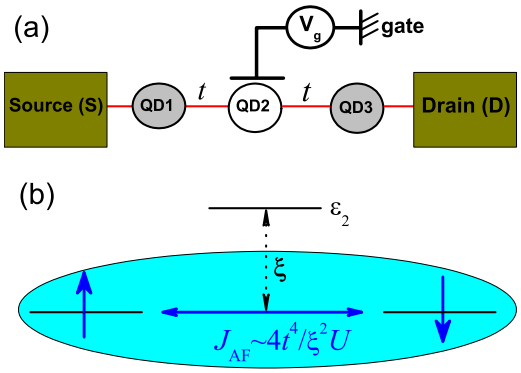

FIG. 1. (a) The schematic diagram of the triple-quantum-dot system. In present work, QD1 and 3 are symmetric and both in the localized momentum regime with $N_1 = N_3 = 1$. QD2 is nearly unoccupied with a gate-modulated on-site energy $\varepsilon_2 = -U/2 + eV_g$. (b) The schematic diagram is shown for the long-range antiferromagnetic exchange interaction ($J_{\rm AF}$) between QD1 and 3 via high-order tunneling processes.

work, as schematically shown in Fig. 1(b), we will demonstrate a long-range antiferromagnetic exchange interaction ($J_{\rm AF} > 0$), which can be simply expressed in terms of $J_{\rm AF} \approx 4t^4/\xi^2 U$, where $\xi \equiv \varepsilon_2 - \varepsilon_1$ (ε_1 being the on-site energy of QD1) is called the detuning energy, and U ($U_i = U; i = 1,2,3$) is the on-dot Coulomb interaction. The effect of $J_{\rm AF}$ on Kondo features including spectral characteristics and Kondo current in TQDs will be discussed in detail.

II. MODEL AND THEORY

The total Hamiltonian for the system is described by the three-impurity Anderson model

$$H = H_{\rm dots} + H_{\rm res} + H_{\rm coup}, \tag{1}$$

where the isolated TQD part is

$$H_{\rm dots} = \sum_{\sigma,i=1,2,3} [\epsilon_{i\sigma}\hat{a}^\dagger_{i\sigma}\hat{a}_{i\sigma} + U n_{i\sigma}n_{i\bar{\sigma}}] + t\sum_{\sigma}(\hat{a}^\dagger_{1\sigma}\hat{a}_{2\sigma} + \hat{a}^\dagger_{2\sigma}\hat{a}_{3\sigma} + {\rm H.c.}), \tag{2}$$

with $\hat{a}^\dagger_{i\sigma}$ ($\hat{a}_{i\sigma}$) being the operator that creates (annihilates) a spin-σ electron with energy $\epsilon_{i\sigma}$ in ith QD. $n_{i\sigma} = \hat{a}^\dagger_{i\sigma}\hat{a}_{i\sigma}$ is the operator of the occupation number.

In what follows, the symbol μ is adopted to denote the electron orbital (including spin, space, etc.) in the system for brevity, i.e., $\mu = \{\sigma, i, \ldots\}$. The device reservoirs are treated as single-particle systems with the Hamiltonian as $H_{\rm res} = \sum_{k\mu\alpha={\rm S,D}} \epsilon_{k\alpha}\hat{d}^\dagger_{k\mu\alpha}\hat{d}_{k\mu\alpha}$, with $\epsilon_{k\alpha}$ being the energy of an electron with wave vector k in the α reservoir, and $\hat{d}^\dagger_{k\mu\alpha}(\hat{d}_{k\mu\alpha})$ the corresponding creation (annihilation) operator for an electron with the α-reservoir state $|k\rangle$ of energy $\epsilon_{k\alpha}$. The Hamiltonian of the dot-reservoir coupling is $H_{\rm coup} = \sum_{k\mu\alpha} t_{k\mu\alpha}\hat{a}^\dagger_\mu\hat{d}_{k\mu\alpha} + {\rm H.c.}$ To describe the stochastic nature of the transfer coupling, it can be written in the reservoir $H_{\rm res}$-interaction picture as $H_{\rm coup} = \sum_\mu [f^\dagger_\mu(t)\hat{a}_\mu + \hat{a}^\dagger_\mu f_\mu(t)]$, with $f^\dagger_\mu = e^{iH_{\rm res}t}[\sum_{k\alpha} t^*_{k\mu\alpha}\hat{d}^\dagger_{k\mu\alpha}]e^{-iH_{\rm res}t}$ being the stochastic interactional operator and satisfying the Gauss statistics. Here, $t_{k\mu\alpha}$ denotes the transfer coupling matrix element. The influence of electron reservoirs on the dots is taken into account through the hybridization functions, which assume Lorentzian form, $\Delta_\alpha(\omega) \equiv \pi\sum_k t_{\alpha k\mu}t^*_{\alpha k\mu}\delta(\omega - \epsilon_{k\alpha}) = \Delta W^2/[2(\omega - \mu_\alpha)^2 + W^2]$, where Δ is the effective quantum dot–reservoir coupling strength, W is the bandwidth, and μ_α is the chemical potentials of the α reservoir.

In this paper, the three-impurity Anderson model is accurately solved by the HEOM approach, which is established based on the Feynman-Vernon path-integral formalism with a general Hamiltonian, in which the system-environment correlations are fully taken into consideration [28,29]. The HEOM formalism is in principle accurate and applicable to arbitrary electronic systems, including Coulomb interactions, under the influence of arbitrary applied bias voltage and external fields. The outstanding issue of characterizing both equilibrium and nonequilibrium properties of a general open quantum system is referred to Refs. [28–33]. It has been demonstrated that the HEOM approach achieves the same level of accuracy as the latest high-level numerical renormalization group and quantum Monte Carlo approaches for the prediction of various dynamical properties at equilibrium and nonequilibrium [29].

The reduced density matrix of the quantum dot system $\rho^{(0)}(t) \equiv {\rm tr}_{\rm res}[\rho_{\rm total}(t)]$ and a set of auxiliary density matrices $\{\rho^{(n)}_{j_1\cdots j_n}(t); n = 1, \ldots, L\}$ are the basic variables in HEOM. L denotes the truncated tier level. The equations governing the dynamics of open systems are in the form of [28,29]

$$\dot{\rho}^{(n)}_{j_1\cdots j_n} = -\left(i\mathcal{L} + \sum_{r=1}^{n}\gamma_{j_r}\right)\rho^{(n)}_{j_1\cdots j_n} - i\sum_j \mathcal{A}_{\bar{j}}\,\rho^{(n+1)}_{j_1\cdots j_n j} - i\sum_{r=1}^{n}(-)^{n-r}\,\mathcal{C}_{j_r}\,\rho^{(n-1)}_{j_1\cdots j_{r-1}j_{r+1}\cdots j_n}, \tag{3}$$

where $\mathcal{A}_{\bar{j}}$ and $\mathcal{C}_{j_r}$ are Grassmannian superoperators which are illustrated in detail in Refs. [28,29].

The dynamical quantities can be acquired via the HEOM-space linear response theory [34]. The spectral function $A(\omega)$ exhibiting prominent Kondo signatures at low temperatures can be evaluated by a half Fourier transformation of correlation functions as

$$A_\mu(\omega) = \frac{1}{\pi}{\rm Re}\left(\int_0^\infty dt\{\tilde{\mathcal{C}}_{\hat{a}^\dagger_\mu\hat{a}_\mu}(t) + [\tilde{\mathcal{C}}_{\hat{a}_\mu\hat{a}^\dagger_\mu}(t)]^*\}e^{i\omega t}\right). \tag{4}$$

The electric current from the α reservoir to the system is given by

$$I_\alpha(t) = i\sum_\mu {\rm tr}_s[\rho^\dagger_{\alpha\mu}(t)\hat{a}_\mu - \hat{a}^\dagger_\mu\rho^-_{\alpha\mu}(t)], \tag{5}$$

where $\rho^\dagger_{\alpha\mu} = (\rho^-_{\alpha\mu})^\dagger$ is the first-tier auxiliary density operator. The details of the HEOM formalism and the derivation of physical quantities are supplied in Refs. [28,29].

III. RESULTS AND DISCUSSION

As shown in Fig. 1, we assume that QD1 and 3 always keep electron-hole symmetry and their parameters are the same, in which $\varepsilon_1 = \epsilon_1 = -U/2$ and $\varepsilon_3 = \epsilon_3 = -U/2$. In order to figure out whether there may exist a long-range exchange

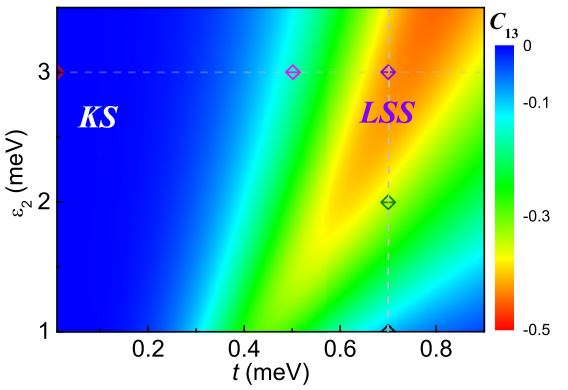

FIG. 2. The spin-spin correlation function $C_{13} \equiv \langle \vec{S}_1 \cdot \vec{S}_3 \rangle - \langle \vec{S}_1 \rangle \cdot \langle \vec{S}_3 \rangle$ varies as a function of the on-site energy of QD2, i.e., ε_2, and the nearest interdot coupling strength t. Two phases are shown: the Kondo singlet (KS, $C_{13} \sim 0$) and long-range spin singlet (LSS, $C_{13} < 0$). The horizontal dashed line marks the gradual change of phases from KS to LSS, which is further elucidated by the spectral functions of the scatter points (see Fig. 3). The vertical dashed line marks the gradual change of phases with ε_2 at $t = 0.7$ meV. The parameters are as follows: $U = 1.2$ (in units of meV), $\epsilon_1 = \epsilon_3 = -0.6$, the bandwidth of reservoirs $W = 5.0$, the temperature $K_B T = 0.03$, and the hybridization width between reservoirs and QDs is $\Delta = 0.3$.

interaction, we calculate the spin-spin correlation function between QD1 and 3,

$$C_{13} \equiv \langle \vec{S}_1 \cdot \vec{S}_3 \rangle - \langle \vec{S}_1 \rangle \cdot \langle \vec{S}_3 \rangle. \tag{6}$$

In Fig. 2, we depict C_{13} as a function of the modulated on-site energy of QD2 ($\varepsilon_2 = \epsilon_2 + eV_g$) and the nearest interdot coupling strength t. The other parameters are as follows: the on-dot Coulomb correlation $U = 1.2$ (in unit of meV), the bandwith of reservoirs $W = 5.0$, the temperature $K_B T = 0.03$ which is much lower than the Kondo temperature of QD1 or 3 derived from the analytical formula in the literature [15], and the hybridization widths between reservoirs and QDs $\Delta = 0.3$. In present work, we set $\varepsilon_2 > 1.0$ meV to keep the configuration of (1,0,1). Two phases are shown in the figure. The first one is the Kondo singlet (KS) which is characterized by near zero correlation between $\vec{S}_1$ and $\vec{S}_3$ ($C_{13} \sim 0$) at small t. The second one is the main finding of the present work, called the long-range spin singlet (LSS) characterized by finite C_{13} ($C_{13} < 0$ in the figure), which proves that a long-range exchange interaction between $\vec{S}_1$ and $\vec{S}_3$ dose exist although direct coupling between them is absent. From the sign of C_{13}, we conclude that the long-range exchange is antiferromagnetic and thus we suggest an effective interaction term as

$$H_{13} = J_{\rm AF} \vec{S}_1 \cdot \vec{S}_3. \tag{7}$$

It is expected that H_{13} plays an important role in quantum computing, which can expand the original idea of the exchange-based quantum gates [5], by manipulating a distant quantum gate or qubit in one step. We comment that the small value of C_{13} in the bottom right corner of Fig. 2 results from the competition between the LSS phase and the effective ferromagnetic phase we have reported in Ref. [30].

More detailed information of the phase diagram in Fig. 2 can be illustrated by the spectral functions $A_{i\sigma}(\omega)$ in different phases. The spin degeneracy makes $A_{i\uparrow}(\omega) = A_{i\downarrow}(\omega) = A_i(\omega)$ and the symmetry in our model also suggests $A_1(\omega) = A_3(\omega)$. We select three characteristic points at $t = 0.01$, 0.5, and 0.7 meV along the dashed line in Fig. 2 at $\varepsilon_2 = 3.0$ ($\xi = 3.6$) meV, and depict their corresponding $A_i(\omega)$ in Figs. 3(a) to 3(c). By referring to Figs. 2 and 3, we find in the limit of weak interdot coupling ($t < 0.2$ meV) the absence of long-range correlation ($C_{13} \sim 0$) results in the individual screening of local momentums by the nearest reservoirs; thus the degenerate KS state is formed. The spectral function $A_1(\omega)/A_3(\omega)$ shows similar behavior to that in a single QD with one Kondo peak at $\omega = 0$, while $A_2(\omega) \sim 0$ around $\omega = 0$ due to the empty occupation, as shown in Fig. 3(a). With the increase of the interdot coupling, the single peak of $A_1(\omega)/A_3(\omega)$ grows slightly higher due to the "t-enhanced Kondo phenomenon" (figure not shown) [31].

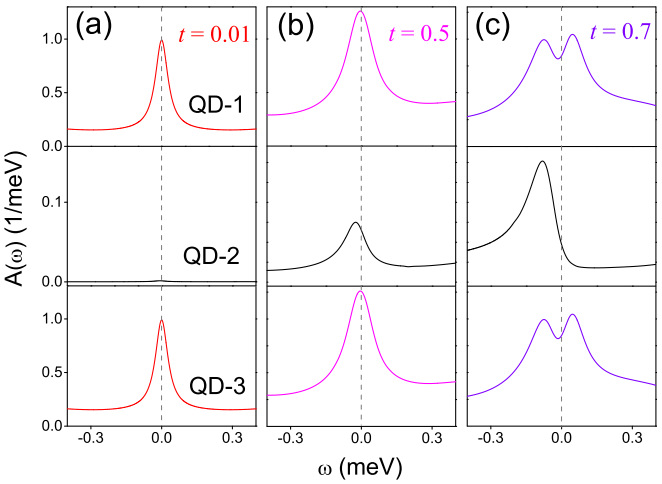

FIG. 3. The spectral functions $A_i(\omega)$ of the TQDs are shown at $\varepsilon_2 = 3.0$ (in unit of meV, $\xi = 3.6$) for different interdot coupling strengths along the horizontal line in Fig. 2: (a) $t = 0.01$, (b) $t = 0.5$, and (c) $t = 0.7$. The top panel: $i = 1$; the middle panel: $i = 2$; and the bottom panel: $i = 3$. The other parameters are the same as those in Fig. 2.

Further increasing t to $t > 0.3$ meV distinctly changes the Kondo features. As shown in Fig. 3(b), the central peak of $A_1(\omega)/A_3(\omega)$ becomes much higher and wider at $t = 0.5$ meV than that at $t = 0.01$ meV; meanwhile a small peak develops in $A_2(\omega)$ near $\omega = 0$. The latter is unusual, since QD2 is still empty and the emerging peak impossibly results from Kondo screening directly. The most possible mechanism is the long-range tunneling between QD1 and 3 by the aid of $J_{\rm AF}$, or equivalently speaking, the electron wave functions separately localized in QD1 and 3 at $t \sim 0$ becomes overlapping within QD2 now. At first glance, it is analogous to the ordinary double-well model in the textbooks; however, what are localized in QD1 and 3 here are not ordinary electrons but Kondo quasiparticles. This means that the Kondo quasiparticle in QD1 can tunnel to QD3 through QD2, via overlapping their wave functions which are nothing but the widely studied "Kondo cloud" [35]. Although we cannot present the spatial distribution of Kondo clouds here, we have demonstrated their long-range overlapping, or long-range quantum entanglement [36].

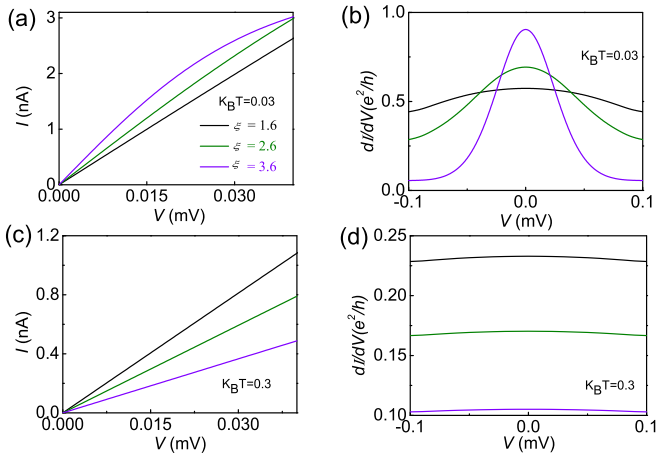

FIG. 4. The I-V curves of the TQD system at various detuning energies ξ at $t = 0.7$ (in units of meV) along the vertical line in Fig. 2 at (a) low temperature $K_BT = 0.03$, and (c) high temperature $K_BT = 0.3$. The corresponding differential conductance dI/dV-V curves at (b) low temperature $K_BT = 0.03$ and (d) high temperature $K_BT = 0.3$. The other parameters are the same as those in Fig. 2.

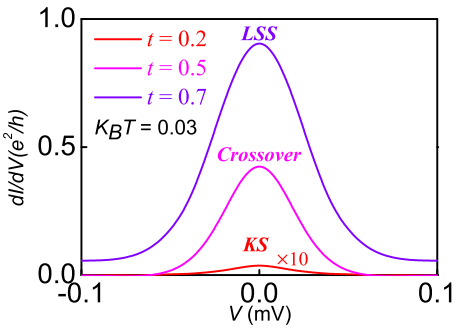

FIG. 5. The differential conductance dI/dV-V curves of the TQD system at $\xi = 3.6$ (in units of meV) for different phases along the horizontal line in Fig. 2: KS ($t = 0.2$), crossover region ($t = 0.5$), and LSS ($t = 0.7$). The other parameters are the same as those in Fig. 2.

In the limit of strong interdot couplings, e.g., $t = 0.7$ meV, the overlapping of Kondo clouds of QD1 and 3 becomes much stronger to induce a distinct peak in $A_2(\omega)$; meanwhile the long-range $J_{\rm AF}$ has induced the crossover from the degenerate KS state of individual QD to the LSS state (see Fig. 2), characterized by the splitting of the Kondo peaks of QD1 and 3 in Fig. 3(c). Since Kondo clouds are hard to be observed in experiments [35], we suggest that they can be captured by their long-range overlapping or entanglement.

In order to relate to experiments and highlight the effect of long-range entanglement of Kondo clouds under nonequilibrium conditions, we then calculate the current-voltage (I-V) curves and corresponding differential conductances dI/dV at various detuning energy ξ at $t = 0.7$ meV and summarize the results respectively in Figs. 4(a) and 4(b) at low temperature $K_BT = 0.03$. Interestingly, we find that current can increase with the increase of ξ, or with the increase of the height of the potential barrier. For example, the current at $V = 0.02$ mV increases from 1.3 nA at $\xi = 1.6$ meV to 2.0 nA at $\xi = 3.6$ meV, as shown in Fig. 4(a). Meanwhile, a conductance peak at zero bias develops with the increase of ξ, as shown in Fig. 4(b). The anomalous enhancement of transport ability obviously results from the long-range entanglement of Kondo clouds. At $t = 0.7$ and $\xi = 3.6$ meV, the long-range entanglement of the Kondo clouds is strong enough to form an extended conductive channel (see Fig. 3); thus the electrons can transfer through QD1 to 3 along this channel no matter how high the barrier in QD2, which induces the enhancement of current and the development of conductance peak at zero bias.

The long-range transport with the aid of the entanglement of Kondo clouds is a many-body effect that is distinctly different from the low-order sequential tunneling and cotunneling. That point can be verified by checking the transport properties at temperature higher than the Kondo temperature, as shown in Figs. 4(c) and 4(d), which depicts the I-V and dI/dV-V curves with the same parameters as those in Figs. 4(a) and 4(b) except $K_BT = 0.3$ meV. Now, the current decreases normally with the increase of ξ or with the increase of the height of the barrier. Of course, no conductance peak can be seen any more [Fig. 4(c)], and all of the dI/dV-V curves become flat with the values of conductance much smaller [Fig. 4(d)] than those shown in Fig. 4(b).

In order to verify the conclusion that the long-range entanglement of the Kondo clouds is characterized by the conductance peak at zero bias, we calculate the dI/dV-V curves at $\xi = 3.6$ meV in different phases along the horizontal line in Fig. 2: KS ($t = 0.2$ meV), crossover region ($t = 0.5$ meV), and LSS ($t = 0.7$ meV). The results are shown in Fig. 5, where the scale of the value of dI/dV of the KS phase is expanded by a factor of 10. As shown in the figure, at small t (KS phase), although the Kondo peaks in QD1 and 3 contribute a possible conductive channel, the high barrier of QD2 prevents the transfer of electrons from QD1 to QD3. Increasing t to 0.5 meV drives the TQDs into the crossover region between KS and LSS. The weak entanglement of Kondo clouds [see Fig. 3(b)] can assist the tunneling of electrons and introduce a conductance peak $\sim 0.4e^2/h$ at zero bias, as shown in Fig. 5. Further increasing t will broaden and heighten the conductance peak. In the LSS phase at $t = 0.7$ meV, the conductance peak at zero bias increases to a much higher value $\sim 0.9e^2/h$ (see Fig. 5) due to the strong entanglement of Kondo clouds [see Fig. 3(c)]. We confirm the maximum value of the conductance peak only accessible in the LSS phase. If one drags the phase out of the LSS by changing t or ε_2 from the top right corner of Fig. 2, the peak will shrink and decrease (figures not shown).

Finally, we will derive an analytical expression of $J_{\rm AF}$ for isolated TQDs, and then prove it is also valid in the open TQD system over a wide range of parameters. We start from the Hamiltonian of Eq. (2) for isolated TQDs and constrain our derivation in the subspace with a total occupation number of $N_T \equiv N_1 + N_2 + N_3 = 2$. The states of double occupation in QD2 (with zero occupation in QD1 and 3, i.e., the $|0,2,0\rangle$ states) are excluded because their energy is much higher than others. When $t = 0$, $E_{|1,0,1\rangle} = 2\epsilon_1$, $E_{|2,0,0\rangle} = E_{|0,0,2\rangle} = 2\epsilon_1 + U$, and $E_{|1,1,0\rangle} = E_{|0,1,1\rangle} = 2\epsilon_1 + \xi$. Since only low-energy states are concerned, we substitute high-energy eigenvalues with their unperturbed ones and solve the secular equation to obtain the singlet and triplet states, where their splitting are defined

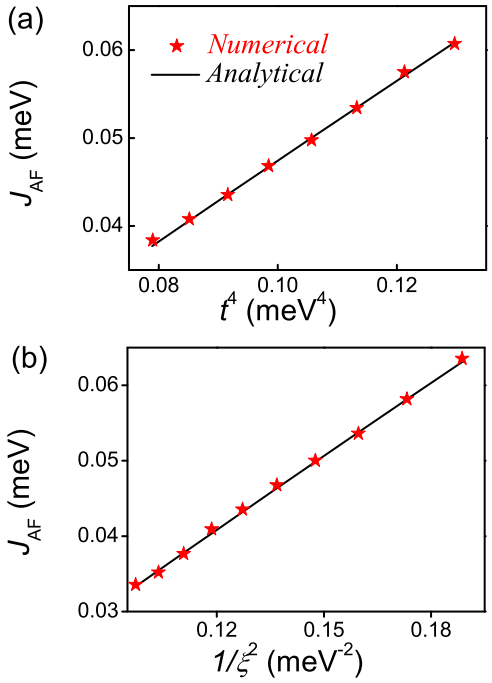

FIG. 6. The dependence of the long-range antiferromagnetic exchange interaction $J_{\rm AF}$ on t^4 and $1/\xi^2$ is calculated in (a) and (b), respectively. The other parameters are $U = 1.2$ and $\xi = 2.6$ in (a), $t = 0.55$ and $U = 1.2$ in (b). The black lines and red scattered points are calculated by the analytic formula [Eq. (8)] and numerical HEOM approach, respectively. The other parameters are the same as those in Fig. 2.

as $J_{\rm AF} \equiv E_T - E_S$. After some algebra and assuming $t \ll U$, we get

$$J_{\rm AF} \approx \frac{4t^4}{\xi^2 U}. \tag{8}$$

Equation (8) is similar to the antiferromagnetic exchange interaction in double QDs (DQDs) if one defines an effective next-neighbor interdot coupling between QD1 and 3 as $t' = t^2/\xi$ to rewrite Eq. (8) as $J_{\rm AF} \approx 4t'^2/U$. However, a rigorous proof is required for open TQD systems. By investigating the splitting of Kondo peaks of QD1 or 3, the features of $J_{\rm AF}$ can be studied, as in DQD systems [29]. The distance between the splitting peaks should equal to $2J_{\rm AF}$.

The results of HEOM calculations on the formula of $J_{\rm AF}$ are summarized in Fig. 6, where $\varepsilon_2 = 2.0$ meV is chosen. The other parameters are the same as those in Fig. 2 unless specified otherwise. The numerical $J_{\rm AF}$ as functions of t^4 and $1/\xi^2$ are respectively shown in Figs. 6(a) and 6(b), together with the analytical results obtained from Eq. (8) for comparison. One can see that almost all of the numerical data fall in the analytical lines in the range of parameters explored here. We thus conclude that $J_{AF} \approx 4t^4/\xi^2 U$ is also valid in open TQD systems over a wide range of parameters. We emphasize some features shown in Fig. 6 as follows: (i) The t^4 dependence shown in Fig. 6(a) indicates that $J_{\rm AF}$ in TQDs is more sensitive to t; thus a larger t is required to induce the crossover from the KS to the LSS phase (cf. Fig. 2). (ii) The $1/\xi^2$ dependence shown in Fig. 6(b) suggests an easy way to manipulate $J_{\rm AF}$ in TQDs via gate control of the detuning energy. In this sense, the phase diagram shown in Fig. 2 is experimentally accessible.

It is well acknowledged that the nearest-neighbor antiferromagnetic exchange can induce a non-Fermi-liquid quantum critical point in DQDs, which is called the "two-impurity problem." Let us make some comments on the relation between the results here and those in DQDs in the literature. In the two-impurity problem, Sela and Affleck found a crossover from the critical point to the low-energy Fermi liquid phase at finite temperature [37]. The quantum phase transition has ever been proved to be very robust against both the asymmetry of the device (parity) and electron-hole asymmetry [38]. That crossover behavior has been verified by our HEOM calculations on parallel-coupled DQDs [29], as well as on serial-coupled ones. For nonequilibrium transport, the HEOM calculations have found the zero-bias conductance peak exhibits a single peak for the weak interdot coupling t. With the increase of t, the zero-bias conductance peak also shows a continuous evolution from single to double peaked behavior. Those nonequilibrium characteristics confirm the conclusions and predictions in Refs. [37,38] and other relevant references. For the TQDs with an unoccupied middle dot as studied here, although the long-range antiferromagnetic exchange is similar to that of DQDs if an effective next-neighbor interdot coupling defined, the characteristics in the strong-coupling limit are quite different. As shown in Fig. 4(b), the zero-bias conductance peak rather than a splitting dip (see Ref. [29]) develops at low temperature. Even at high temperature, the dip character will not appear as shown in Fig. 4(d). Therefore, the HEOM calculations have revealed new nonequilibrium transport characteristics in TQDs, which can improve the understandings in the above-mentioned literature, including our work.

IV. SUMMARY

In summary, we have investigated the long-range interactions in triple quantum dots (TQDs) in the Kondo regime, by accurately solving the three-impurity Anderson model with the hierarchical equation of motion (HEOM) formalism. For the occupation configuration of $(N_1,N_2,N_3) = (1,0,1)$, we demonstrate that there exists a long-range antiferromagnetic exchange interaction, $J_{\rm AF}$, which can induce a crossover from the separated Kondo singlet (KS) to the long-range spin singlet (LSS) state between edge dots. In the LSS phase, a long-range overlapping or entanglement of Kondo clouds is discovered, which induces a transition peak in the spectral function of the middle dot under equilibrium conditions. Under nonequilibrium conditions, the long-range entanglement of Kondo clouds induces an anomalous enhancement of current and a conductance peak at zero bias, which can be observed in experiments. The expression of $J_{\rm AF} \approx 4t^4/\xi^2 U$ is analytically derived and numerically verified, according to which $J_{\rm AF}$ can be conveniently manipulated via gate control of the detuning energy.

ACKNOWLEDGMENTS

This work was supported by the NSF of China (No. 11374363) and the Research Funds of Renmin University

of China (Grant No. 11XNJ026). Computational resources have been provided by the Physical Laboratory of High Performance Computing at Renmin University of China. Z.G.Z. is supported by the Hundred Talents Program of CAS.

[1] Philip Richerme, Zhe-Xuan Gong, Aaron Lee, Crystal Senko, Jacob Smith, Michael Foss-Feig, Spyridon Michalakis, Alexey V. Gorshkov, and Christopher Monroe, Nature (London) **511**, 198 (2014).
[2] Pawel Szumniak, Jaroslaw Pawlowski, Stanislaw Bednarek, and Daniel Loss, Phys. Rev. B **92**, 035403 (2015).
[3] F. R. Braakman, P. Barthelemy, C. Reichl, W. Wegscheider, and L. M. K. Vandersypen, Nat. Nanotechnol. **8**, 432 (2013).
[4] Rafael Sánchez, Fernando Gallego-Marcos, and Gloria Platero, Phys. Rev. B **89**, 161402 (2014).
[5] D. Loss and D. P. DiVincenzo, Phys. Rev. A **57**, 120 (1998).
[6] L. Gaudreau, S. A. Studenikin, A. S. Sachrajda, P. Zawadzki, A. Kam, J. Lapointe, M. Korkusinski, and P. Hawrylak, Phys. Rev. Lett. **97**, 036807 (2006).
[7] D. Schröer, A. D. Greentree, L. Gaudreau, K. Eberl, L. C. L. Hollenberg, J. P. Kotthaus, and S. Ludwig, Phys. Rev. B **76**, 075306 (2007).
[8] G. Granger, L. Gaudreau, A. Kam, M. Pioro-Ladriere, S. A. Studenikin, Z. R. Wasilewski, P. Zawadzki, and A. S. Sachrajda, Phys. Rev. B **82**, 075304 (2010).
[9] M. C. Rogge and R. J. Haug, Phys. Rev. B **77**, 193306 (2008).
[10] A. Mühle, W. Wegscheider, R. J. Haug *et al.*, Appl. Phys. Lett. **92**, 013126 (2008).
[11] S. Amaha, T Hatano, T. Kubo *et al.*, Appl. Phys. Lett. **94**, 092103 (2009).
[12] M. Busl, G. Granger, L. Gaudreau, R. Sánchez, A. Kam, M. Pioro-Ladrière, S. A. Studenikin, P. Zawadzki, Z. R. Wasilewski, A. S. Sachrajda, and G. Platero, Nat. Nanotechnol. **8**, 261 (2013).
[13] R. Sánchez, G. Granger, L. Gaudreau, A. Kam, M. Pioro-Ladrière, S. A. Studenikin, P. Zawadzki, A. S. Sachrajda, and G. Platero, Phys. Rev. Lett. **112**, 176803 (2014).
[14] J. Kondo, Prog. Theor. Phys. **32**, 37 (1964).
[15] A. C. Hewson, *The Kondo Problem to Heavy Fermions* (Cambridge University Press, Cambridge, 1993).
[16] T. K. Ng and P. A. Lee, Phys. Rev. Lett. **61**, 1768 (1988).
[17] Zhao-tan Jiang, Qing-feng Sun, and Yupeng Wang, Phys. Rev. B **72**, 045332 (2005).
[18] Rok Žitko and Janez Bonča, Phys. Rev. Lett. **98**, 047203 (2007).
[19] T. Kuzmenko, K. Kikoin, and Y. Avishai, Europhys. Lett. **64**, 218 (2003).
[20] P. P. Baruselli, R. Requist, M. Fabrizio, and E. Tosatti, Phys. Rev. Lett. **111**, 047201 (2013).
[21] T. Kuzmenko, K. Kikoin, and Y. Avishai, Phys. Rev. B **73**, 235310 (2006).
[22] E. Vernek, P. A. Orellana, and S. E. Ulloa, Phys. Rev. B **82**, 165304 (2010).
[23] Takahide Numata, Yunori Nisikawa, Akira Oguri *et al.*, Phys. Rev. B **80**, 155330 (2009).
[24] M. N. Kiselev, K. Kikoin, and J. Richert, Phys. Rev. B **81**, 115330 (2010).
[25] A. Oguri, S. Amaha, Y. Nishikawa, T. Numata, M. Shimamoto, A. C. Hewson, and S. Tarucha, Phys. Rev. B **83**, 205304 (2011).
[26] Rosa Lopez, Tomaz Rejec, Jan Martinek *et al.*, Phys. Rev. B **87**, 035135 (2013).
[27] A. Deb, J. M. Ralph, E. J. Cairns, and U. Bergmann, Phys. Rev. B **73**, 115114 (2006).
[28] J. S. Jin, X. Zheng, and Y. J. Yan, J. Chem. Phys. **128**, 234703 (2008).
[29] ZhenHua Li, NingHua Tong, Xiao Zheng, Dong Hou, JianHua Wei, Jie Hu, and YiJing Yan, Phys. Rev. Lett. **109**, 266403 (2012).
[30] Yongxi Cheng, JianHua Wei, and YiJing Yan, Europhys. Lett. **112**, 57001 (2015).
[31] Yongxi Cheng, WenJie Hou, YuanDong Wang, ZhenHua Li, JianHua Wei, and YiJing Yan, New J. Phys. **17**, 033009 (2015).
[32] J. S. Jin, S. K. Wang, X. Zheng, and Y. J. Yan, J. Chem. Phys. **142**, 234108 (2015).
[33] Y. J. Yan, J. Chem. Phys. **140**, 054105 (2014).
[34] J. H. Wei and Y. J. Yan, arXiv:1108.5955.
[35] I. Affleck, arXiv:0911.2209.
[36] S.-S. B. Lee, Jinhong Park, and H.-S. Sim, Phys. Rev. Lett. **114**, 057203 (2015).
[37] Eran Sela and Ian Affleck, Phys. Rev. Lett. **102**, 047201 (2009).
[38] Gergely Zaránd, Chung-Hou Chung, Pascal Simon, and Matthias Vojta, Phys. Rev. Lett. **97**, 166802 (2006).